energies

MDPI

Article

CO_2 and CH_4 Adsorption Behavior of Biomass-Based Activated Carbons

Deneb Peredo-Mancilla [1,2,*], Imen Ghouma [3], Cecile Hort [2], Camelia Matei Ghimbeu [3], Mejdi Jeguirim [3] and David Bessieres [1]

1 CNRS/Total/Univ Pau & Pays Adour/ E2S UPPA, Laboratoire des Fluides Complexes et Leurs Reservoirs-IPRA, UMRS5150, 64000 Pau, France; david.bessieres@univ-pau.fr
2 Univ Pau & Pays Adour/ E2S UPPA, Laboratoire de Thermique, Energetique et Procedes-IPRA, EA1932, 64000 Pau, France; cecile.hort@univ-pau.fr
3 Institut de Sciences des Matériaux de Mulhouse, UMR 7661 CNRS, 15 rue Jean Starcky, 68057 Mulhouse, France; imenghouma83@gmail.com (I.G.); camelia.ghimbeu@uha.fr (C.M.G.); mejdi.jeguirim@uha.fr (M.J.)
* Correspondence: peredo-mancilla.jd@univ-pau.fr

Received: 25 July 2018; Accepted: 8 November 2018; Published: 13 November 2018

check for updates

Abstract: The aim of the present work is to study the effect of different activation methods for the production of a biomass-based activated carbon on the CO_2 and CH_4 adsorption. The influence of the activation method on the adsorption uptake was studied using three activated carbons obtained by different activation methods (H_3PO_4 chemical activation and H_2O and CO_2 physical activation) of olive stones. Methane and carbon dioxide pure gas adsorption experiments were carried out at two working temperatures (303.15 and 323.15 K). The influence of the activation method on the adsorption uptake was studied in terms of both textural properties and surface chemistry. For the three adsorbents, the CO_2 adsorption was more important than that of CH_4. The chemically-activated carbon presented a higher specific surface area and micropore volume, which led to a higher adsorption capacity of both CO_2 and CH_4. For methane adsorption, the presence of mesopores facilitated the diffusion of the gas molecules into the micropores. In the case of carbon dioxide adsorption, the presence of more oxygen groups on the water vapor-activated carbon enhanced its adsorption capacity.

Keywords: CO_2 adsorption; CH_4 adsorption; biomass; activated carbon

1. Introduction

As part of the efforts being made to fight climate change, governments of 195 countries signed the Paris Agreement, in which they agreed to keep the increase of the global average temperature well below 2 °C from the preindustrial temperatures [1]. In order to meet this target, the EU set a 20-20-20 goal: 20% increase of energy efficiency, 20% reduction of greenhouse gas (GHG) emissions and 20% of EU energy from renewables by 2020. Furthermore, 10% of transportation fuels have to come from renewable sources such as biofuels [2].

Biogas is a gaseous mixture produced when organic matter is degraded by micro-organisms under anaerobic conditions in a process known as anaerobic digestion (AD); its main components are methane (CH_4) in a concentration of 50–70 vol% and carbon dioxide (CO_2) ranging from 30–45 vol% Collected biogas can be directly burned to produce electricity with an efficiency of roughly 38% [3]. Alternatively, the energy density of biogas can be increased by an upgrading process in which the non-combustible gas (CO_2) and other impurities are separated to produce biomethane, a highly-purified methane stream (around 98% purity), which can function as a vehicle fuel or can also be injected into the natural gas grid.

The use of biogas and biomethane as alternative energy sources has gained attention, because it results in the reduction of greenhouse gases from both the burning of fossil fuels and from the landfill of organic wastes, which accounts for 3.2% of the total GHG emissions of the EU. Consequently, in Europe, more than 90% of the produced biogas is already being used for electricity generation, and the upgrading of biogas is being promoted more and more [4]. EU energy production from biomethane rose from 752 GWh in 2011 to 17.264 GWh in 2016 (+16.512 GWh). Moreover, in 2016, biomethane production in Europe increased by 4.971 GWh (+40%), proving an accelerated development in the sector [5].

Adsorption-based processes have been widely explored for the upgrading of biogas. They present several advantages such as relatively low energy requirements and low capital investment costs, flexibility of design, safety and simplicity of operation, as well as a high separation efficiency [6]. In this type of separation technology, the components of a gas mixture are separated by their molecular characteristics and affinity to an adsorbent material. For this purpose, a variety of materials have been studied including zeolites [7–9], carbon molecular sieves (CMS) [10–12], metal organic frameworks (MOFs) [13–15] and activated carbons (ACs) [16–18]. Among these materials, activated carbons present advantages in terms of: (i) hydrophobicity; thus, there is no need for a drying step before upgrading; (ii) low heat of adsorption, therefore a low energy of regeneration; (iii) the possibility of heteroatoms' functionalization to modify their adsorption behavior; and (iv) high CO_2 adsorption capacity at ambient pressure [19]. Furthermore, activated carbons can be produced with a lower cost than other adsorbents, with a wide range of available precursor materials. In fact, any carbonaceous material can be used as a precursor for activated carbon production as long as it has a low ash content and a high proportion of carbon [20]. In this sense, the use of agro-industrial wastes as an alternative to coal and wood as precursors for activated carbon production has been widely studied [21–23]. This waste-valorization process reduces the environmental and economic costs associated with the precursors while eliminating the need for disposal or incineration of unwanted agricultural by-products [24]. Materials such as corn cobs, palm shells, starch, coconut shells, durian shell, olive stones and bamboo have already been studied for activated carbon production [19,25–32]. In particular, olive stones are seen as suitable precursors, giving activated carbon with high adsorption capacities, important mechanical strength and low ash content [29,33]. A complete review of precursors, activation methods and applications of biomass-based activated carbons is available elsewhere [34].

Depending on the activation conditions, ACs can present surface areas as high as 3000 $m^2\ g^{-1}$. Activated carbons can be produced in two ways: physical activation and chemical activation. Physical activation is a two-step process that begins with the carbonization of the precursor at high temperatures (up to 1073 K), a process in which the volatile compounds present in the precursor are removed under an inert atmosphere (i.e., nitrogen atmosphere) producing a carbon-rich material. Carbonization is followed by the activation step: the material is exposed to an oxidizing gas current (such as air, CO_2 and water vapor) at a temperature between 1073 and 1273 K. On the other hand, chemical activation consists of the immersion of the raw material into a dehydrating agent followed by a heat treatment step. Examples of dehydrating agents are sodium and potassium hydroxide (KOH and NaOH), zinc chloride ($ZnCl_2$) and phosphoric acid (H_3PO_4). Chemical activation with KOH results in activated carbons with a high micropore volume, a key factor for CH_4 and CO_2 adsorption; nevertheless, this activation agent presents the disadvantage of low production yields due to the presence of potassium atoms on the resulting structure, which lowers the activated carbon yield; thus, the carbon content of the obtained activated carbon is lower than that of the precursor material. The use of ZnCl as the activation agent has environmental disadvantages due to zinc chloride's high corrosivity. Therefore, H_3PO_4 has become the most used impregnation agent for AC production [35].

Different activation methods and activation conditions (i.e., temperature and time of activation) result in differences in the textural properties such as surface area, pore size distribution and micropore volume, as well as in the chemical properties of the obtained activated carbons. The textural properties are the most determining factor of the adsorption behavior in a physical adsorption process.

However, specific interactions between the adsorbed gas and the adsorbent may also play a role in the adsorption process, and they are unique for each adsorbent/adsorbate pair [36]. Therefore, it is necessary to establish the best activation method for each particular adsorption process.

Several studies have been published on the CH_4 and CO_2 adsorption capacity of CO_2 physically-activated carbon, as well as KOH chemically-activated carbons, but a less important number of works report H_3PO_4 activation [19,25,31,35,37–42]. The literature review shows that the use of olive stones as precursor materials for activated carbon production is a promising alternative for biogas upgrading with the additional advantage of waste valorization. In this context, the present work provides a novel systematic analysis of the influence of both the textural properties and surface chemistry of olive stone activated carbons on the methane and carbon dioxide adsorption. The effect of the activation method (physical versus chemical activation) on the properties of the obtained activated carbons is also discussed. To this end, the adsorption capacity of both methane and carbon dioxide is determined for three activated carbons produced from olive stones by different activation methods: CO_2 physical activation, H_2O physical activation and H_3PO_4 chemical activation. The factors influencing the gas adsorption capacity are discussed in terms of the effect of the activation method on both the textural and chemical properties of the obtained activated carbon.

2. Materials

2.1. Sample Preparation

Three activated carbons were prepared using olive stones provided by an olive oil factory located in Zarzis (Tunisia); two of them were obtained by physical activation and the other one by chemical activation. Prior to the activation procedures, the raw materials, were thoroughly washed with hot distilled water, dried under ambient conditions for 24 h and crushed to form particles with a diameter between 1 and 3 mm. The activated carbon preparation methods are summarized in this section. A detailed description of the selection procedure of the optimal activation conditions and sample characterization can be found in [43–45].

2.1.1. Physical Activation

Two physical activation methods were carried out: activation with water vapor and activation with carbon dioxide. Both methods followed a two-step scheme in which the first step was the carbonization of the precursor under a continuous flow of purified nitrogen with a flow rate of 10 NL/h. Using a heating velocity of 5 K/min, the precursor was heated from room temperature to a temperature of 873 K and kept at this final temperature for 60 min. Nitrogen flow was used in order to evacuate the residual oxygen from the system. The second step was the activation of the samples consisting of placing the sample under a gas flow of the activation agent at a flow velocity of 10 Nl/h and a temperature of 1023 K for 360 min (temperature ramp of 15 K/min). For the water vapor activated carbon (AC-H_2O), the activation agent was water 70 vol. % in N_2. Meanwhile, for CO_2 activation, a flow of pure carbon dioxide was employed.

2.1.2. Chemical Activation

The olive stones were immersed in an orthophosphoric acid aqueous solution (50% w/w) at a weight ratio of 1:3. The mixture was kept under stirring for 9 h at 383 K. Consecutively, the solution was filtrated, dried and flushed by a stream of nitrogen at a temperature of 443 K for 30 min and an extra 150 min at 683 K. The heating velocity during this whole procedure was 5 K/min. The sample, referred to as AC-H_3PO_4, had a chemical activation yield of 33 wt%.

2.2. Samples Properties

The characterization of the activated carbons was done by means of textural properties (such as surface area and pore volume) and surface chemistry. The specific surface area was calculated by means of the Brunauer–Emmett–Teller (BET) method [46] from the linear plot of the nitrogen adsorption isotherm at 77 K in the relative pressure range of 0.05–0.15 (Figure S1 of the Supplementary Materials). Total pore volume was determined by the amount of nitrogen adsorbed by each material at a relative pressure P/P° = 0.99. The *t*-plot method was used for the calculation of the micropore volume. The mesopore volume was defined as the difference between the total pore volume and the micropore volume. Finally, the pore size distribution (PSD) (Figure S2 of the Supplementary Materials) was obtained by non-local density functional theory (NLDFT) using a model for slit carbon pores. The textural properties of the three activated carbons are summarized in Table 1 and can also be found in the literature [43]. The three activated carbons are mainly microporous. The water vapor activated carbon has a higher total pore volume V_{TOT} due to the presence of an important volume of mesopores (V_{meso} = 0.30 cm^3 g^{-1}). The presence of mesopores on water vapor-activated carbons due to a higher gasification of the carbon source of the precursor has been previously reported [43,47]. On the other hand, the chemically-activated carbon AC-H_3PO_4 has significantly higher specific surface area (SSA) and micropore volume V_μ than the physically-activated ones, in agreement with the literature [48].

Table 1. Textural properties of carbon materials. *SSA*, specific surface area; AC, activated carbon.

Sample	SSA (m^2 g^{-1})	V_μ (cm^3 g^{-1})	V_{TOT} (cm^3 g^{-1})	V_{meso} (cm^3 g^{-1})
AC-H_3PO_4	1178	0.45	0.49	0.04
AC-CO_2	757	0.30	0.32	0.02
AC-H_2O	754	0.28	0.58	0.30

The surface chemistry of the adsorbent can be of great importance for the adsorption process; for this reason, the type and quantity of surface oxygenated groups were determined by means of a home-made temperature programmed desorption device coupled with a mass spectrometer (TPD-MS). In the TPD-MS experiments, a sample weighting 10 mg of each activated carbon was placed in a quartz tube that was introduced to an oven. The temperature of the oven was then increased at a rate of 5 K per minute under vacuum conditions. The surface properties of the sample were analyzed in the temperature range 298–1173 K. During the heating process, the quantitative evolution of gases was analyzed by mass spectrometry. The total amount of emitted CO and CO_2 during the TPD-MS analysis was obtained by integration of the desorption peaks (see Table 2). With the increase of temperature, oxygenated groups decomposed into CO_2 and CO. The desorption temperature gives information about the nature of oxygenated groups present on the carbon surface. Furthermore, by correlation between diffuse reflectance infrared Fourier transform spectroscopy (DRIFTS) spectra of different activated carbons and their TPD-MS profiles, it has been established that the emission of carbon dioxide results from the decomposition of lactones, carboxylic acids and anhydrides, while carbon monoxide is emitted by the decomposition of groups such as phenols, ethers and quinones [49].

Table 2. Cumulated amounts of the emitted CO and CO_2 during the temperature programmed desorption (TPD-MS) analysis of carbon materials.

Sample	CO (mmol g^{-1})	CO_2 (mmol g^{-1})
AC-H_3PO_4	3.43	0.72
AC-CO_2	1.06	0.38
AC-H_2O	1.25	0.39

In this context, the chemically-activated carbon (AC-H_3PO_4) presented higher amounts of oxygenated groups, mainly carboxylic acids, quinones and anhydrides. Among the physically-activated carbons, the water vapor activation resulted in more surface oxygen in the form of phenol and carboxylic acids. Meanwhile, carbon dioxide activation resulted in the formation of quinones, lactones and carboxylic acids on the activated carbon surface [43].

3. Experimental Methodology

3.1. High Pressure Manometric Adsorption Setup

The instrument used in the present study was a high pressure (HP) manometric device. A schematic view of this "homemade" apparatus is provided in Figure 1. The fundamental elements of this apparatus are the dosing cell (V_{dos}) and the adsorption cell (V_{ads}). The pressure was measured by a MKS pressure transducer Baratron Type 121 A MKS Instruments, München, Deutschland). (0.01% uncertainty in the full scale from vacuum to 3.3 MPa) connected to the dosing cell. The two cells were isolated by spherical valves, thus limiting the "dead space" volume. During the adsorption experiments, the isothermal condition of the system was ensured by a heating wire controlled by a Eurotherm 3208 PID. (Schneider Electric, Worthing, United Kingdom). Thermocouples located at several points of the instrument allowed verifying the non-appearance of temperature gradients within the system. This setup was designed to operate over wide a range of pressure (0–3.3 MPa) and temperature up to 373.15 K [50,51].

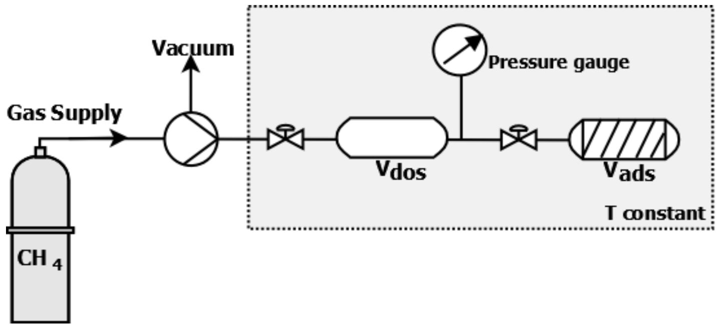

Figure 1. Schematic diagram of the high pressure and high temperature (HP/HT) manometric adsorption setup.

3.2. Determination of Excess Adsorption

Prior to the adsorption experiments, both the dossing cell volume and adsorption cell volume need to be calculated. The volume of the dosing cell was measured by a gravimetric scheme in which the pressure change at a given temperature due to a known quantity of carbon dioxide (CO_2) was recorded, using the NIST isothermal properties of carbon dioxide, the corresponding volume was calculated [52]. The adsorption cell accessible volume, also known as void volume, in the presence of the sample of activated carbon was calculated by helium (He) expansions from the dossing cell to the adsorption cell (helium is considered as a non-sorbing gas). The experimental methodology applied for the adsorption isotherms' measurement was based on a mass balance principle. The uncertainty in the calculations of the void and adsorption cell volume was always less than 0.5%. In all cases, an out-gassing process consisting of keeping the sample under vacuum conditions at 473 K for 10 h was performed before any experiment. The adsorption isotherms were obtained by an accumulative process: successive doses (≈3 bar) of the adsorbate (CH_4 or CO_2) were introduced into the dosing cell and expanded into the adsorption cell. The stability of the pressure was the chosen indicator of equilibrium conditions. The reproducibility of the experiment was tested by repeating one of the adsorption isotherm 3 times, and the absolute standard deviation was found to be less than 1%.

3.3. Parametrization of Excess Adsorption Isotherms

The excess adsorption isotherms were fitted to a modified Langmuir model:

$$n_{exc} = n_L \frac{p}{p + p_L} \left(1 - \frac{\rho_g(p, T)}{\rho_{ads}} \right) \quad (1)$$

In this expression, n_{exc} represents the adsorbed amount of gas (mol kg^{-1}) at a pressure p (MPa); p_L is the pressure at which half of the adsorption sites are occupied (monolayer), also known as the Langmuir pressure; n_L is the maximum Langmuir capacity, which corresponds to the adsorbed amount in which the monolayer is filled; ρ_g is the gas density (kg m^{-3}) at pressure p and temperature T. Meanwhile, ρ_{ads} (kg m^{-3}) stands for the adsorbed phase density; in this work, it was fixed to the inverse of the van der Waals volume of each gas (373 kg m^{-3} for methane and 1027 kg m^{-3} for carbon dioxide) [53]. The Langmuir model has the advantage of taking into account the volume of the adsorbed phase. It has a theoretical basis, whilst other models such as Toth (1995) [54] and Sips (1948) [55] are empirical. This model was initially developed for the low pressure region; nevertheless, it provides a reasonable estimation of the excess adsorption isotherms at higher pressures [17].

The best fit of the Langmuir model for each adsorption isotherm was obtained by minimizing the root mean square error ($RMSE$) provided by Equation (2) [7]:

$$RMSE = \frac{1}{k} \cdot \sqrt{\sum_{1}^{k} (n_{exp} - n_{calc})^2} \tag{2}$$

where n_{exp} and n_{calc} are the experimental and calculated adsorption amounts in mol kg^{-1} at a pressure p for a number k of data points in the adsorption isotherm.

4. Results

CH_4 and CO_2 adsorption isotherms were obtained for the set of three olive stone-based activated carbons (Figures 2 and 3) up to a pressure of 3.2 MPa at two working temperatures: 303.15 and 323.15 K, with a reproducibility superior to 99% (average absolute deviation of less than 1%). All the isotherms were fitted by the Langmuir two-parameter model (see Equation (1)), and the obtained fitting parameters and root mean square error ($RMSE$) are presented in Table 3 (CH_4 adsorption) and Table 4 (CO_2 adsorption). The goodness of the fitting process is depicted by the $RMSE$ values; values under 0.09 were obtained for the fitting of all the isotherms.

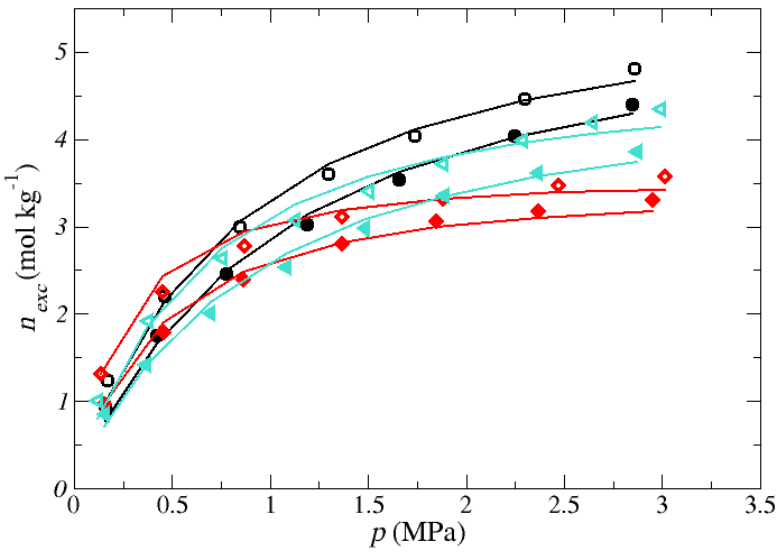

Figure 2. CH_4 adsorption isotherms for the three olive stone-based activated carbons: AC-H_3PO_4 (black circles), AC-CO_2 (red diamonds) and AC-H_2O (turquoise triangles). Open symbols represent the adsorption data at 303.15 K, while the data at 323.15 are shown by the filled symbols. Uncertainties: Δp = 0.01 MPa, ΔT = 0.2 K. The obtained Langmuir fitting isotherms are shown by the solid lines.

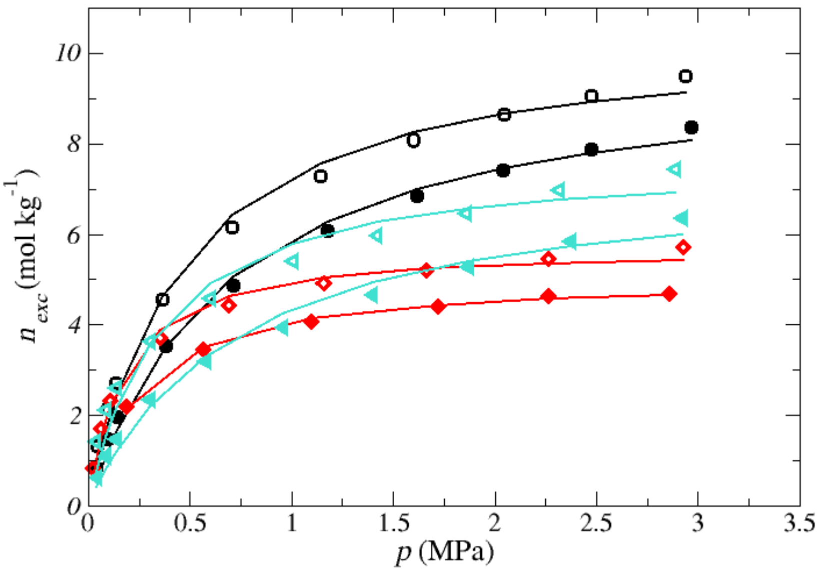

Figure 3. CO_2 adsorption isotherms for the three olive stone-based activated carbons: AC-H_3PO_4 (black circles), AC-CO_2 (red diamonds) and AC-H_2O (turquoise triangles). Open symbols represent the adsorption data at 303.15 K, while the data at 323.15 are shown by the filled symbols. Uncertainties: Δp = 0.01 MPa, ΔT = 0.2 K. The obtained Langmuir fitting isotherms are shown by the solid lines.

A higher adsorption of carbon dioxide than methane can be noticed for the three ACs (Figures 2 and 3). This is a typical behavior of activated carbon adsorption that can be explained by the presence of a quadrupole moment on the molecule of carbon dioxide that leads to stronger adsorptive/adsorbent interactions. Another possible explanation can be given in terms of the critical point of the gases: the critical temperature (190 K) and critical pressure (4.59 MPa) of methane were much lower than those of carbon dioxide (304.45 K and 7.38 MPa), which means that carbon dioxide was in the form of a condensable vapor, while methane acted as a supercritical gas at the adsorption conditions. A lower adsorption and lower maximum Langmuir capacity (n_L) upon an increase in the adsorand Tables 3 and 4, indicating a physical adsorption process. Furthermore, for both adsorptives, the chemically-activated carbon AC-H_3PO_4 showed a higher adsorption capacity; the adsorption tendency varied in the following order: AC-H_3PO_4 > AC-H_2O > AC-CO_2.

Table 3. Langmuir fitting parameters for the CH_4 adsorption isotherms.

CH_4 Adsorption				
Sample	**Temperature (K)**	n_L **(mol kg^{-1})**	ρ_L **(MPa)**	***RMSE***
AC-H_3PO_4	303.15 323.15	6.518 6.369	0.932 1.182	0.042 0.037
AC-CO_2	303.15 323.15	3.913 3.830	0.273 0.076	0.043 0.031
AC-H_2O	303.15 323.15	5.417 5.301	0.714 1.011	0.067 0.056

The superior adsorption of AC-H_3PO_4 can be explained in regards to the textural properties of the samples (see Table 1); the chemically-activated carbon had the highest specific surface area and micropore volume, both adsorption-enhancing factors. A higher surface area means more available physisorption sites, while a linear relationship between the micropore volume and the adsorption of both methane and carbon dioxide has been reported [21,56]. Concerning the difference in the methane adsorption capacity of the two physically-activated carbons, the presence of the mesoporosity of the structure of the water vapor-activated carbon AC-H_2O is thought to be the determining factor. Both physically-activated carbons had similar *SSA* and micropore volume, with the only difference being the mesopore volume. In fact, it has been shown that activated carbons that combine both micropores and mesopores can adsorb a significantly higher amount of CH_4 than their totally microporous counterparts [57].

Table 4. Langmuir fitting parameters for the CO_2 adsorption isotherms.

CO_2 Adsorption				
Sample	**Temperature (K)**	n_L **(mol kg^{-1})**	ρ_L **(MPa)**	***RMSE***
AC-H_3PO_4	303.15	10.873	0.488	0.080
	323.15	10.254	0.733	0.065
AC-CO_2	303.15	5.878	0.181	0.059
	323.15	5.191	0.273	0.020
AC-H_2O	303.15	7.968	0.371	0.073
	323.15	7.721	0.772	0.087

While methane adsorption by activated carbons is only influenced by the textural properties of the adsorbent, the carbon dioxide adsorption is also thought to be related to the surface chemistry. In the present work, the influence of the surface chemistry was depicted by normalizing the CO_2 adsorption isotherms by the surface area (Figure 4). One could expect that by doing this, the adsorption of the chemically-activated carbon would still be the most important due to a higher micropore volume. In reality, the AC-H_2O showed a higher adsorption. Chemical activation with phosphoric acid (H_3PO_4) was reported to produce acid activated carbon surfaces [58], which seems to reduce the interactions between the basic surface groups and the carbon dioxide molecules, explaining its lower adsorption when the textural effect is eliminated by normalizing the adsorption isotherms by the specific surface area. However, the negative influence of acid surface groups on the AC-H_3PO_4 was small compared to the effect of its higher surface area, thus showing a higher adsorption capacity when no normalization of the isotherms was done (Table 4).

Among the two physically-activated carbons, AC-H_2O had the highest quantity of oxygenated surface groups (Table 2), which explains its dominant adsorption when *SSA* normalized. An increase in the CO_2 adsorption capacity in the presence of oxygen-containing surface functionalities by means of acid-base interactions and hydrogen bond formation between the adsorbate and the activated carbons surface was shown [59,60]. The high electronic density of oxygen on the oxygenated surface groups, due to electron gain from the carbon surface atoms, allowed them to act as electron-donors, in which case the CO_2 adsorbate molecules behaved as basic groups.

Table 5 shows the comparison of the adsorption capacities of the activated carbons studied in this work with other biomass-based activated carbons of the literature. It can be seen that the adsorption values were well in the range reported in the literature for both carbon dioxide and methane. Their competitive adsorption capacities and higher carbon dioxide adsorption capacity over methane made the olive stone activated carbons a suitable material for further studies on the CH_4 and CO_2 storage and separation.

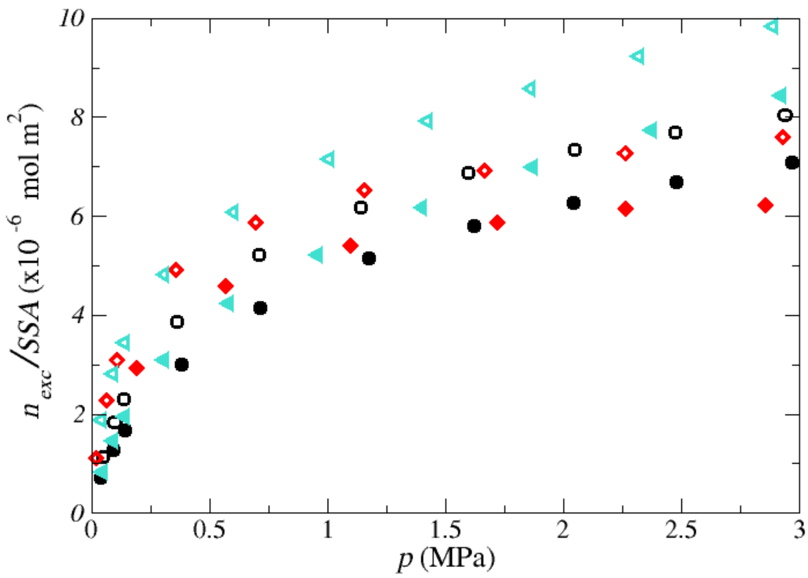

Figure 4. *SSA* normalized CO_2 adsorption isotherms of the activated carbons: AC-H_3PO_4 (black circles), AC-CO_2 (red diamonds) and AC-H_2O (turquoise triangles). Open symbols represent the adsorption data at 303.15 K, while the data at 323.15 are shown by the filled symbols 323.15 K.

Table 5. Adsorption capacities of different biomass-based adsorbents.

CO_2 and CH_4 Adsorption Capacity					
Sample	**Precursor**	**Activation Agent**	**Temperature (K)**	**CH_4 Adsorption Capacity (mol kg^{-1})**	**CO_2 Adsorption Capacity (mol kg^{-1})**
AC-H_3PO_4 *	Olive stones	H_3PO_4	303.15	6.518	10.873
AC-CO_2 *	Olive stones	CO_2	303.15	3.913	5.878
AC-H_2O *	Olive stones	H_2O *	303.15	5.417	7.968
BC [19]	Babassu coconut	CO_2	293	5.343	10.49
CS [19]	Coconut shell	CO_2	293	7.259	14.67
Pinpel20 [61]	Wood pellets	CO_2	303	3.36	6.66
MSS-AC [62]	Mango Seeds	H_3PO_4	303	0.858	8.788
CS-H_2O [39]	Cherry stones	H_2O	303	8.36	14.45

* This work.

5. Conclusions

In this work, the effects of the textural and chemical properties of three activated carbons on the adsorption behavior of carbon dioxide and methane were studied. For this purpose, three activated carbons produced from olive stones by CO_2 physical activation, H_2O physical activation and H_3PO_4 chemical activation were employed. The activated carbons were mainly microporous. The activated carbon obtained by chemical activation with phosphoric acid of the precursor material presents a higher surface area, total pore volume and micropore volume, which led to a higher adsorption capacity for both methane and carbon dioxide. Even though the two physically-activated carbons had similar surface areas and micropore volume, the water vapor-activated carbon had also an important volume of mesopores that facilitated the diffusion of the methane molecules into the micropores; thus, its methane adsorption capacity was higher. In the case of carbon dioxide, adsorption-specific interactions between the adsorptive and adsorbent were also found to participate in the adsorption process. Amongst the two physically-activated carbons, H_2O-activated carbon had the highest content of oxygen surface group and therefore a higher CO_2 adsorption capacity. Nevertheless, even if the surface chemistry of the adsorbents can influence the adsorption of carbon dioxide, textural properties are still the main governing parameters. Finally, the three activated carbons from olive stones had a higher adsorption of carbon dioxide than methane, meaning a higher selectivity towards carbon dioxide than methane. Furthermore, their carbon dioxide and methane adsorption capacities were found to be in the range of other biomass-based activated carbons reported in the literature, making them suitable candidates for the upgrading of biogas.

Supplementary Materials: The following are available online at http://www.mdpi.com/1996-1073/11/11/3136/s1, Figure S1: Adsorption and desorption of nitrogen (N2) at 77 K on the olive stone activated carbons. Figure S2: Pore size distribution (PSD) of the olive stone activated carbons obtained by means of density functional theory (DFT). Figure S3: Emitted CO_2 during temperature programmed desorption-mass spectroscopy (TPD-MS) of the olive stone activated carbons. Figure S4: Emitted CO during temperature programmed desorption-mass spectroscopy (TPD-MS) of the olive stone activated carbons.

Author Contributions: Sample preparation and characterization: I.G., C.M.G. and M.J. Adsorption isotherms: D.P.-M., C.H. and D.B. Writing of the article: D.P.-M. Revision of the article content: All of the authors.

Funding: This research received no external funding

Acknowledgments: Deneb Peredo is grateful to CONACyT for the fellowship 293897 to pursue her PhD degree.

Conflicts of Interest: The authors declare no conflict of interest.

References

1. European Comission. Paris Agreement. Available online: https://ec.europa.eu/clima/policies/international/negotiations/paris_en (accessed on 12 November 2018)
2. European Comission. Renewable Energy. Moving towards a low carbon economy. Available online: https://ec.europa.eu/energy/en/topics/renewable-energy (accessed on 12 November 2018)
3. Starr, K.; Villalba, G.; Gabarrell, X. Upgraded biogas from municipal solid waste for natural gas substitution and CO_2 reduction—A case study of Austria, Italy, and Spain. *Waste Manag.* **2015**, *38*, 105–116, doi:10.1016/j.wasman.2015.01.001. [CrossRef] [PubMed]
4. Sahota, S.; Shah, G.; Ghosh, P.; Kapoor, R.; Sengupta, S.; Singh, P.; Vijay, V.; Sahay, A.; Vijay, V.K.; Thakur, I.S. Review of trends in biogas upgradation technologies and future perspectives. *Bioresour. Technol. Rep.* **2018**, *1*, 79–88, doi:10.1016/j.biteb.2018.01.002. [CrossRef]
5. EBA European Biogas Association. EBA Statictical Report 2017 Published Soon. Available online: http://european-biogas.eu/2017/12/14/eba-statistical-report-2017-published-soon/ (accessed on 12 November 2018)
6. Angelidaki, I.; Treu, L.; Tsapekos, P.; Luo, G.; Campanaro, S.; Wenzel, H.; Kougias, P.G. Biogas upgrading and utilization: Current status and perspectives. *Biotechnol. Adv.* **2018**, *36*, 452–466, doi:10.1016/j.biotechadv.2018.01.011. [CrossRef] [PubMed]
7. Jiang, Y.; Ling, J.; Xiao, P.; He, Y.; Zhao, Q.; Chu, Z.; Liu, Y.; Li, Z.; Webley, P.A. Simultaneous biogas purification and CO_2 capture by vacuum swing adsorption using zeolite NaUSY. *Chem. Eng. J.* **2018**, *334*, 2593–2602, doi:10.1016/j.cej.2017.11.090. [CrossRef]
8. Gong, H.; Lee, S.S.; Bae, T.H. Mixed-matrix membranes containing inorganically surface-modified 5A zeolite for enhanced CO_2/CH_4 separation. *Microporous Mesoporous Mater.* **2017**, *237*, 82–89, doi:10.1016/j.micromeso.2016.09.017. [CrossRef]
9. Kennedy, D.A.; Tezel, F.H. Cation exchange modification of clinoptilolite—Screening analysis for potential equilibrium and kinetic adsorption separations involving methane, nitrogen, and carbon dioxide. *Microporous Mesoporous Mater.* **2018**, *262*, 235–250, doi:10.1016/j.micromeso.2017.11.054. [CrossRef]
10. Son, S.J.; Choi, J.S.; Choo, K.Y.; Song, S.D.; Vijayalakshmi, S.; Kim, T.H. Development of carbon dioxide adsorbents using carbon materials prepared from coconut shell. *Korean J. Chem. Eng.* **2005**, *22*, 291–297, doi:10.1007/BF02701500. [CrossRef]
11. Rocha, L.A.; Andreassen, K.A.; Grande, C.A. Separation of CO_2/CH_4 using carbon molecular sieve (CMS) at low and high pressure. *Chem. Eng. Sci.* **2017**, *164*, 148–157, doi:10.1016/j.ces.2017.01.071. [CrossRef]
12. Arya, A.; Divekar, S.; Rawat, R.; Gupta, P.; Garg, M.O.; Dasgupta, S.; Nanoti, A.; Singh, R.; Xiao, P.; Webley, P.A. Upgrading biogas at low pressure by vacuum swing adsorption. *Ind. Eng. Chem. Res.* **2015**, *54*, 404–413, doi:10.1021/ie503243f. [CrossRef]
13. Samarasinghe, S.A.; Chuah, C.Y.; Yang, Y.; Bae, T.H. Tailoring CO_2/CH_4 separation properties of mixed-matrix membranes via combined use of two- and three-dimensional metal-organic frameworks. *J. Membr. Sci.* **2018**, *557*, 30–37, doi:10.1016/j.memsci.2018.04.025. [CrossRef]

14. Zacharia, R.; Gomez, L.F.; Chahine, R.; Cossement, D.; Benard, P. Thermodynamics and kinetics of CH_4/CO_2 binary mixture separation by metal-organic frameworks from isotope exchange and adsorption break-through. *Microporous Mesoporous Mater.* **2018**, *263*, 165–172, doi:10.1016/j.micromeso.2017.12.011. [CrossRef]
15. Cheng, Y.; Wang, X.; Jia, C.; Wang, Y.; Zhai, L.; Wang, Q.; Zhao, D. Ultrathin mixed matrix membranes containing two-dimensional metal-organic framework nanosheets for efficient CO_2/CH_4 separation. *J. Membr. Sci.* **2017**, *539*, 213–223, doi:10.1016/j.memsci.2017.06.011. [CrossRef]
16. Yao, K.X.; Chen, Y.; Lu, Y.; Zhao, Y.; Ding, Y. Ultramicroporous carbon with extremely narrow pore distribution and very high nitrogen doping for efficient methane mixture gases upgrading. *Carbon* **2017**, *122*, 258–265, doi:10.1016/j.carbon.2017.06.073. [CrossRef]
17. Koonaphapdeelert, S.; Moran, J.; Aggarangsi, P.; Bunkham, A. Low pressure biomethane gas adsorption by activated carbon. *Energy Sustain. Dev.* **2018**, *43*, 196–202, doi:10.1016/j.esd.2018.01.010. [CrossRef]
18. Saha, D.; Nelson, K.; Chen, J.; Lu, Y.; Ozcan, S. Adsorption of CO_2 ,CH_4, and N_2 in Micro-Mesoporous Nanographene: A Comparative Study. *J. Chem. Eng. Data* **2015**, *60*, 2636–2645, doi:10.1021/acs.jced.5b00291. [CrossRef]
19. Vilella, P.C.; Lira, J.A.; Azevedo, D.C.; Bastos-Neto, M.; Stefanutti, R. Preparation of biomass-based activated carbons and their evaluation for biogas upgrading purposes. *Ind. Crops Prod.* **2017**, *109*, 134–140, doi:10.1016/j.indcrop.2017.08.017. [CrossRef]
20. Rashidi, N.A.; Yusup, S. An overview of activated carbons utilization for the post-combustion carbon dioxide capture. *J. CO_2 Util.* **2016**, *13*, 1–16, doi:10.1016/j.jcou.2015.11.002. [CrossRef]
21. Serafin, J.; Narkiewicz, U.; Morawski, A.W.; Wróbel, R.J.; Michalkiewicz, B. Highly microporous activated carbons from biomass for CO_2 capture and effective micropores at different conditions. *J. CO_2 Util.* **2017**, *18*, 73–79, doi:10.1016/j.jcou.2017.01.006. [CrossRef]
22. Yadavalli, G.; Lei, H.; Wei, Y.; Zhu, L.; Zhang, X.; Liu, Y.; Yan, D. Carbon dioxide capture using ammonium sulfate surface modified activated biomass carbon. *Biomass Bioenergy* **2017**, *98*, 53–60, doi:10.1016/j.biombioe.2017.01.015. [CrossRef]
23. Hao, W.; Björkman, E.; Lilliestråle, M.; Hedin, N. Activated carbons prepared from hydrothermally carbonized waste biomass used as adsorbents for CO_2. *Appl. Energy* **2013**, *112*, 526–532, doi:10.1016/j.apenergy.2013.02.028. [CrossRef]
24. Gil, R.R.; Ruiz, B.; Lozano, M.S.; Fuente, E. Influence of the pyrolysis step and the tanning process on KOH-activated carbons from biocollagenic wastes. Prospects as adsorbent for CO_2 capture. *J. Anal. Appl. Pyrolysis* **2014**, *110*, 194–204, doi:10.1016/j.jaap.2014.09.001. [CrossRef]
25. Bagheri, N.; Abedi, J. Adsorption of methane on corn cobs based activated carbon. *Chem. Eng. Res. Des.* **2011**, *89*, 2038–2043, doi:10.1016/j.cherd.2011.02.002. [CrossRef]
26. Arami-Niya, A.; Daud, W.M.A.W.; Mjalli, F.S. Comparative study of the textural characteristics of oil palm shell activated carbon produced by chemical and physical activation for methane adsorption. *Chem. Eng. Res. Des.* **2011**, *89*, 657–664, doi:10.1016/j.cherd.2010.10.003. [CrossRef]
27. Alabadi, A.; Razzaque, S.; Yang, Y.; Chen, S.; Tan, B. Highly porous activated carbon materials from carbonized biomass with high CO_2 capturing capacity. *Chem. Eng. J.* **2015**, *281*, 606–612, doi:10.1016/j.cej.2015.06.032. [CrossRef]
28. Chen, Y.; Zhou, L.j.; Hong, Y.z.; Cao, F.; Li, L.; Li, J.b. Preparation of high-surface-area activated carbon from coconut shell fibers. *Carbon* **2010**, *48*, 3005, doi:10.1016/j.carbon.2010.03.059. [CrossRef]
29. Iley, M.; Marsh, H.; Rodriguez-Reinoso, F. The Adsorptive Properties of Carbonised Olive Stones. *Carbon* **1973**, *11*, 633–636, doi:10.1016/0008-6223(73)90330-8. [CrossRef]
30. Zhao, G.; Zou, G.; Hou, H.; Ge, P.; Cao, X.; Ji, X. Sulfur-doped carbon employing biomass-activated carbon as a carrier with enhanced sodium storage behavior. *J. Mater. Chem. A* **2017**, *5*, 24353–24360, doi:10.1039/C7TA07860A. [CrossRef]
31. Yakout, S.M.; Sharaf El-Deen, G. Characterization of activated carbon prepared by phosphoric acid activation of olive stones. *Arab. J. Chem.* **2016**, *9*, S1155–S1162, doi:10.1016/j.arabjc.2011.12.002. [CrossRef]
32. Wei, H.; Deng, S.; Hu, B.; Chen, Z.; Wang, B.; Huang, J.; Yu, G. Granular Bamboo-Derived Activated Carbon for High CO_2 Adsorption: The Dominant Role of Narrow Micropores. *ChemSusChem* **2012**, *5*, 2354–2360, doi:10.1002/cssc.201200570. [CrossRef] [PubMed]

33. Álvarez-Gutiérrez, N.; García, S.; Gil, M.V.; Rubiera, F.; Pevida, C. Towards bio-upgrading of biogas: Biomass waste-based adsorbents. *Energy Procedia* **2014**, *63*, 6527–6533, doi:10.1016/j.egypro.2014.11.688. [CrossRef]
34. González-García, P. Activated carbon from lignocellulosics precursors: A review of the synthesis methods, characterization techniques and applications. *Renew. Sust. Energy Rev.* **2018**, *82*, 1393–1414, doi:10.1016/j.rser.2017.04.117. [CrossRef]
35. Gil, M.V.; Martínez, M.; García, S.; Rubiera, F.; Pis, J.J.; Pevida, C. Response surface methodology as an efficient tool for optimizing carbon adsorbents for CO_2 capture. *Fuel Process. Technol.* **2013**, *106*, 55–61, doi:10.1016/j.fuproc.2012.06.018. [CrossRef]
36. Djeridi, W.; Ben Mansour, N.; Ouederni, A.; Llewellyn, P.L.; El Mir, L. Influence of the raw material and nickel oxide on the CH_4 capture capacity behaviors of microporous carbon. *Int. J. Hydrogen Energy* **2015**, *40*, 13690–13701, doi:10.1016/j.ijhydene.2015.05.010. [CrossRef]
37. Soudani, N.; Najar-Souissi, S.; Abderkader-Fernandez, V.; Ouederni, A. Effects of nitrogen plasma treatment on the surface characteristics of olive stone-based activated carbon. *Environ. Technol.* **2017**, *38*, 956–966, doi:10.1080/09593330.2016.1214626. [CrossRef] [PubMed]
38. Balsamo, M.; Tsyntsarski, B.; Erto, A.; Budinova, T.; Petrova, B.; Petrov, N.; Lancia, A. Dynamic studies on carbon dioxide capture using lignocellulosic based activated carbons. *Adsorption* **2015**, *21*, 633–643, doi:10.1007/s10450-015-9711-7. [CrossRef]
39. Álvarez-Gutiérrez, N.; García, S.; Gil, M.V.; Rubiera, F.; Pevida, C. Dynamic Performance of Biomass-Based Carbons for CO_2/CH_4 Separation. Approximation to a Pressure Swing Adsorption Process for Biogas Upgrading. *Energy Fuels* **2016**, *30*, 5005–5015, doi:10.1021/acs.energyfuels.6b00664. [CrossRef]
40. Erto, A.; Tsyntsarski, B.; Balsamo, M.; Budinova, T.; Lancia, A.; Petrova, B.; Petrov, N. Synthesis of Activated Carbons by Thermal Treatments of Agricultural Wastes for CO_2 Capture from Flue Gas. *Combust. Sci. Technol.* **2016**, *188*, 581–593, doi:10.1080/00102202.2016.1138809. [CrossRef]
41. Moussa, M.; Bader, N.; Querejeta, N.; Durán, I.; Pevida, C.; Ouederni, A. Toward sustainable hydrogen storage and carbon dioxide capture in post-combustion conditions. *J. Environ. Chem. Eng.* **2017**, *5*, 1628–1637, doi:10.1016/j.jece.2017.03.003. [CrossRef]
42. Balsamo, M.; Silvestre-Albero, A.; Silvestre-Albero, J.; Erto, A.; Rodríguez-Reinoso, F.; Lancia, A. Assessment of CO_2 adsorption capacity on activated carbons by a combination of batch and dynamic tests. *Langmuir* **2014**, *30*, 5840–5848, doi:10.1021/la500780h. [CrossRef] [PubMed]
43. Ghouma, I.; Jeguirim, M.; Sager, U.; Limousy, L.; Bennici, S.; Däuber, E.; Asbach, C.; Ligotski, R.; Schmidt, F.; Ouederni, A. The potential of activated carbon made of agro-industrial residues in NOx immissions abatement. *Energies* **2017**, *10*, 508, doi:10.3390/en10101508. [CrossRef]
44. Ghouma, I.; Jeguirim, M.; Dorge, S.; Limousy, L.; Matei Ghimbeu, C.; Ouederni, A. Activated carbon prepared by physical activation of olive stones for the removal of NO_2 at ambient temperature. *Comptes Rendus Chimie* **2015**, *18*, 63–74, doi:10.1016/j.crci.2014.05.006. [CrossRef]
45. Limousy, L.; Ghouma, I.; Ouederni, A.; Jeguirim, M. Amoxicillin removal from aqueous solution using activated carbon prepared by chemical activation of olive stone. *Environ. Sci. Pollut. R.* **2017**, *24*, 9993–10004, doi:10.1007/s11356-016-7404-8. [CrossRef] [PubMed]
46. Brunauer, S.; Emmett, P.H.; Teller, E. Adsorption of Gases in Multimolecular Layers. *J. Am. Chem. Soc.* **1938**, *60*, 309–319. [CrossRef]
47. Román, S.; Ledesma, B.; Álvarez-Murillo, A.; Al-Kassir, A.; Yusaf, T. Dependence of the microporosity of activated carbons on the lignocellulosic composition of the precursors. *Energies* **2017**, *10*, 542, doi:10.3390/en10040542. [CrossRef]
48. Song, T.; Liao, J.M.; Xiao, J.; Shen, L.H. Effect of micropore and mesopore structure on CO_2 adsorption by activated carbons from biomass. *Xinxing Tan Cailiao/New Carbon Mater.* **2015**, *30*, 156–166, doi:10.1016/S1872-5805(15)60181-0. [CrossRef]
49. Figueiredo, J.; Pereira, M.; Freitas, M.; Órfão, J. Modification of the surface chemistry of activated carbons. *Carbon* **1999**, *37*, 1379–1389, doi:10.1016/S0008-6223(98)00333-9. [CrossRef]
50. Ortiz Cancino, O.P.; Peredo Mancilla, D.; Pozo, M.; Pérez, E.; Bessieres, D. Effect of Organic Matter and Thermal Maturity on Methane Adsorption Capacity on Shales from the Middle Magdalena Valley Basin in Colombia. *Energy Fuels* **2017**, *31*, 11698–11709, doi:10.1021/acs.energyfuels.7b01849. [CrossRef]

51. Peredo-Mancilla, D.; Hort, C.; Jeguirim, M.; Ghimbeu, C.M.; Limousy, L.; Bessieres, D. Experimental Determination of the CH_4 and CO_2 Pure Gas Adsorption Isotherms on Different Activated Carbons. *J. Chem. Eng. Data* **2018**, doi:10.1021/acs.jced.8b00297. [CrossRef]
52. National Institute of Standards and Technology NIST, U.S. Secretary of Commerce. Isothermal Properties for Carbon Dioxide. Available online: https://webbook.nist.gov/cgi/cbook.cgi?Name=carbon+dioxide&Units=SI (accessed on 12 November 2018).
53. Gensterblum, Y.; Merkel, A.; Busch, A.; Krooss, B.M. High-pressure CH_4 and CO_2 sorption isotherms as a function of coal maturity and the influence of moisture. *Int. J. Coal Geol.* **2013**, *118*, 45–57, doi:10.1016/j.coal.2013.07.024. [CrossRef]
54. Tóth, J. Uniform interpretation of gas/solid adsorption. *Adv. Colloid Interface Sci.* **1995**, *55*, 1–239, doi:10.1016/0001-8686(94)00226-3. [CrossRef]
55. Sips, R. On the Structure of a Catalyst Surface. *J. Chem. Phys.* **1948**, *16*, 490–495, doi:10.1063/1.1746922. [CrossRef]
56. Lozano-Castelló, D.; Cazorla-Amorós, D.; Linares-Solano, A.; Quinn, D.F. Influence of pore size distribution on methane storage at relatively low pressure: Preparation of activated carbon with optimum pore size. *Carbon* **2002**, *40*, 989–1002, doi:10.1016/S0008-6223(01)00235-4. [CrossRef]
57. Casco, M.E.; Martínez-Escandell, M.; Gadea-Ramos, E.; Kaneko, K.; Silvestre-Albero, J.; Rodríguez-Reinoso, F. High-pressure methane storage in porous materials: Are carbon materials in the pole position? *Chem. Mater.* **2015**, *27*, 959–964, doi:10.1021/cm5042524. [CrossRef]
58. Nowicki, P.; Wachowska, H.; Pietrzak, R. Active carbons prepared by chemical activation of plum stones and their application in removal of NO_2. *J. Hazard. Mater.* **2010**, *181*, 1088–1094, doi:10.1016/j.jhazmat.2010.05.126. [CrossRef] [PubMed]
59. Liu, Y.; Wilcox, J. Molecular Simulation Studies of CO_2 Adsorption by Carbon Model Compounds for Carbon Capture and Sequestration Applications. *Environ. Sci. Technol.* **2013**, *47*, 95–101, doi:10.1021/es3012029. [CrossRef] [PubMed]
60. Xing, W.; Liu, C.; Zhou, Z.; Zhou, J.; Wang, G.; Zhuo, S.; Xue, Q.; Song, L.; Yan, Z. Oxygen-containing functional group-facilitated CO_2 capture by carbide-derived carbons. *Nanoscale Res. Lett.* **2014**, *9*, 1–8, doi:10.1186/1556-276X-9-189. [CrossRef] [PubMed]
61. Vivo-Vilches, J.F.; Pérez-Cadenas, A.F.; Maldonado-Hódar, F.J.; Carrasco-Marín, F.; Faria, R.P.V.; Ribeiro, A.M.; Ferreira, A.F.P.; Rodrigues, A.E. Biogas upgrading by selective adsorption onto CO_2 activated carbon from wood pellets. *J. Environ. Chem. Eng.* **2017**, *5*, 1386–1393, doi:10.1016/j.jece.2017.02.015. [CrossRef]
62. Munusamy, K.; Somani, R.S.; Bajaj, H.C. Breakthrough adsorption studies of mixed gases on mango (*Mangifera indica* L.) seed shell derived activated carbon extrudes. *J. Environ. Chem. Eng.* **2015**, *3*, 2750–2759, doi:10.1016/j.jece.2015.05.010. [CrossRef]